Stem Cell Reports
Article

ISSCR

OPEN ACCESS

Modeling Human Bile Acid Transport and Synthesis in Stem Cell-Derived Hepatocytes with a Patient-Specific Mutation

Hisamitsu Hayashi,[1] Shuhei Osaka,[1] Kokoro Sakabe,[2] Aiko Fukami,[2] Eriko Kishimoto,[2] Eitaro Aihara,[3] Yusuke Sabu,[1] Ayumu Mizutani,[1] Hiroyuki Kusuhara,[1] Nakayuki Naritaka,[2] Wujuan Zhang,[2,3] Stacey S. Huppert,[2,3] Masahide Sakabe,[2] Takahisa Nakamura,[2,3] Yueh-Chiang Hu,[2,3] Christopher Mayhew,[2,3] Kenneth Setchell,[2,3] Takanori Takebe,[2,3,4] and Akihiro Asai[2,3,5,*]

[1]Graduate School of Pharmaceutical Science, The University of Tokyo, Tokyo, Japan
[2]Cincinnati Children's Hospital Medical Center, Cincinnati, OH, USA
[3]College of Medicine, University of Cincinnati, Cincinnati, OH, USA
[4]Institute of Research, Tokyo Medical and Dental University, Tokyo, Japan
[5]Lead Contact
*Correspondence: Akihiro.asai@cchmc.org
https://doi.org/10.1016/j.stemcr.2020.12.008

SUMMARY

The bile salt export pump (BSEP) is responsible for the export of bile acid from hepatocytes. Impaired transcellular transport of bile acids in hepatocytes with mutations in BSEP causes cholestasis. Compensatory mechanisms to regulate the intracellular bile acid concentration in human hepatocytes with BSEP deficiency remain unclear. To define pathways that prevent cytotoxic accumulation of bile acid in hepatocytes, we developed a human induced pluripotent stem cell-based model of isogenic BSEP-deficient hepatocytes in a Transwell culture system. Induced hepatocytes (i-Heps) exhibited defects in the apical export of bile acids but maintained a low intracellular bile acid concentration by inducing basolateral export. Modeling the autoregulation of bile acids on hepatocytes, we found that BSEP-deficient i-Heps suppressed *de novo* bile acid synthesis using the FXR pathway via basolateral uptake and export without apical export. These observations inform the development of therapeutic targets to reduce the overall bile acid pool in patients with BSEP deficiency.

INTRODUCTION

Since bile flow is dependent on efficient bile acid transport by hepatocytes, genetic defects affecting bile acid transporters that disturb the canalicular export of bile acids result in cholestasis. The characteristic pattern of clinical presentation of cholestasis includes jaundice, elevated serum bile acid levels, fat malabsorption, and liver injury (Morotti et al., 2011). Prominent among the subset of genetic diseases are defects in the bile salt export pump (BSEP). Deficiency of this transporter is known to present in several clinical phenotypes: progressive familial intrahepatic cholestasis type 2 (PFIC2), benign recurrent intrahepatic cholestasis type 2, and intrahepatic cholestasis of pregnancy (Strautnieks et al., 1998, 2008). PFIC2, the most severe form, has a wide spectrum of clinical manifestations—most commonly, newborn cholestasis with varying rates of progression of the liver dysfunction (Nicolaou et al., 2012). There are no therapeutic agents that have been found to be significantly effective for the treatment of patients with severe PFIC2 because the specific molecular mechanisms governing the alterations in bile acid homeostasis remain unclear.

Because BSEP is responsible for the excretion of intracellular conjugated bile acids into the bile canaliculus via the apical membrane, it has been suggested that hepatocytes accumulate bile acids intracellularly when BSEP export capacity is impaired. However, direct evidence of exceedingly high concentrations of intracellular bile acid in BSEP-deficient hepatocytes has been sparsely reported. Puzzlingly, in a tumor cell line (HepaRG cells) with BSEP knockdown, the HepaRG cells themselves do not accumulate taurocholic acid (TCA), the main conjugated bile acids in newborns, after importing the exogenous TCA (Qiu et al., 2016). The fate of intracellular bile acids of BSEP-deficient hepatocytes remains ill defined. In healthy hepatocytes, excreted bile acids return to the hepatocytes via the enterohepatic circulation, conducting autocrine regulation on the hepatocytes. The intracellular concentration of bile acids plays a crucial role as a sensor for the hepatocytes to regulate synthesis, reabsorption, and excretion of bile acid and thus determine the overall "pool size" of bile acids circulating in the serum and gastrointestinal tract. In hepatocytes congenitally BSEP deficient due to genomic mutations, it is unknown whether the autoregulated homeostasis can be achieved in the absence of apical export of bile acids and, thus, in a defective enterohepatic bile acid circulation.

To delineate the pathologic and compensatory alterations in BSEP-deficient hepatocytes, several attempts have been made to generate rodent models that can recapitulate the phenotypes observed in patients with PFIC2. In the liver of the BSEP knockout mouse, expression of *ABCB1*/MDR1, a transporter of bile acids at the bile canaliculus, is significantly increased, suggesting one compensatory mechanism to reduce the intracellular bile acid

concentration via canalicular excretion (Wang et al., 2003). However, in an analysis of gene expression of the human liver of patients with PFIC2, this MDR1 compensatory response was not evident (Keitel et al., 2005). Furthermore, since the bile of patients with PFIC2 contains a minimal amount of conjugated bile acids, BSEP-deficient human hepatocytes seemingly lack the compensatory bile acid transporter on the canalicular membrane (Jansen et al., 1999). Therefore, we hypothesized that BSEP-deficient human hepatocytes excrete bile acids back into the sinusoid via basolateral excretion by upregulating alternative transporters.

Simple cultures of human hepatocytes fail to form functional apicobasolateral polarity; thus, it has been difficult to investigate bile acid transport in human hepatocytes due to the lack of a suitable experimental system for the dynamic tracing of transcellular transport of bile acids. Study of *de novo* bile acid synthesis by cultured hepatocytes has been possible only with a primary cell culture of explanted liver. Because an explanted liver from patients with PFIC2 is rarely available, an experimental investigation into the regulatory mechanism of bile acid synthesis and transport in human BSEP-deficient hepatocytes has not been reported. In a previous study using induced pluripotent stem cell (iPSC)-derived hepatocytes, there was a documented defect in bile export in hepatocyte-like cells with BSEP deficiency, although the regulatory mechanism of bile acid transport was not addressed (Imagawa et al., 2017). To overcome this limitation, we used human iPSCs and developed an *in vitro* culture system where iPSCs were differentiated into hepatocyte-like cells on a permeable membrane of a two-chamber (Transwell) system (Asai et al., 2017). Using this system, we investigated the fate of intracellular bile acids and their role as a mediator between *de novo* bile acid synthesis and transcellular transport.

RESULTS

Generation of BSEP/*ABCB11*^{R1090X} Mutant Human iPSCs

We identified one set of siblings who had an identical genotype of *ABCB11*; c.2782C > T (R928X) and c.3268C > T (R1090X). Because their parents were heterozygous for each truncating mutation, the genetic test indicates compound heterozygous mutations. Both siblings presented with severe cholestasis and required liver transplant before the age of 1 year. To investigate the biological impact of a severe mutation in bile acid efflux, we selected the R1090X truncating nonsense mutation, which was reported in previous cases as a homozygous genotype (Strautnieks et al., 1998, 2008). To elucidate the specific effects of the R1090X truncating mutation on the BSEP function in hepatocytes, we used CRISPR-Cas9 genome editing to target the R1090 codon in the BSEP/*ABCB11* gene in iPSCs obtained from a healthy donor (Figures 1A and S1A–S1C). The pluripotency of iPSCs remained comparable in parental and R1090X-edited iPSCs (Figures S1D and S1E). To increase clinical relevance and test if our system models BSEP deficiency in the patient's own genomic background, we also generated iPSCs from peripheral blood cells of one of the siblings. This patient-origin iPSC line underwent the same evaluation for its pluripotency as described above. The iPSC line is labeled as iPSC^{patient}, and its BSEP genotype was BSEP$^{R927X/R1090X}$.

BSEP^{R1090X} iPSCs Differentiate into Hepatocyte-like Cells and Express BSEP Protein in an Altered Pattern

To determine whether the edited iPSCs-BSEP^{R1090X} and iPSCs^{patient} are able to differentiate into hepatocytes, we first induced hepatic differentiation with the same method as with the parental iPSCs with normal BSEP (iPSCs-BSEP^{normal} or normal iPSCs). To quantify the efficiency of the hepatic differentiation, we measured the albumin secretion of induced hepatocytes (i-Heps). The BSEP^{R1090X} hepatocytes (BSEP^{R1090X} i-Heps) and BSEP^{patient} hepatocytes (BSEP^{patient} i-Heps) exhibited albumin secretion into the culture medium comparable to that of the normal i-Heps (Figure 1B). Most of the albumin was secreted into the lower chamber (Figure 1B, left). The number of cells in a well and albumin production per cell were comparable between normal cells, BSEP^{R1090X} i-Heps, and BSEP^{patient} i-Heps (Figure 1B, right, and Figure S2A). To determine hepatocytes' metabolic function, we measured CYP3A4 activity and inducibility. i-Heps were incubated with rifampicin for 2 days and BSEP^{R1090X} i-Heps exhibited induced activity of CYP3A4 comparable to that of normal i-Heps (Figure S2B). All i-Heps showed polygonal hepatocyte-like cells (Figure 1C). At the final stage of the differentiation protocol, BSEP^{R1090X} i-Heps and BSEP^{patient} i-Heps expressed hepatic differentiation markers (HNF4a, CPS1) and tight-junction protein 1 (ZO1) in a pattern comparable to that of normal i-Heps (Figures 1D and S2C). A morphometric analysis of HNF4a^{+} cells showed highly efficient hepatic differentiation (>90%) in all i-Heps (Figure S2D). To determine the pattern of cellular polarity, we performed co-immunostaining of i-Heps with F-actin (relatively concentrated on the canalicular membrane of hepatocytes in the human liver tissue), Na-K transporting ATPase a1 (ATP1A1; expressed on the basolateral membrane in hepatocytes), and ZO1 (expressed between the canalicular and the basolateral membrane) and analyzed their z-stack confocal images. F-actin was detected mainly on the apical membrane in normal cells, BSEP^{R1090X} i-Heps, and BSEP^{patient} i-Heps, with a lower degree of expression on the lateral membrane (Figure 1E). ATP1A1 was detected

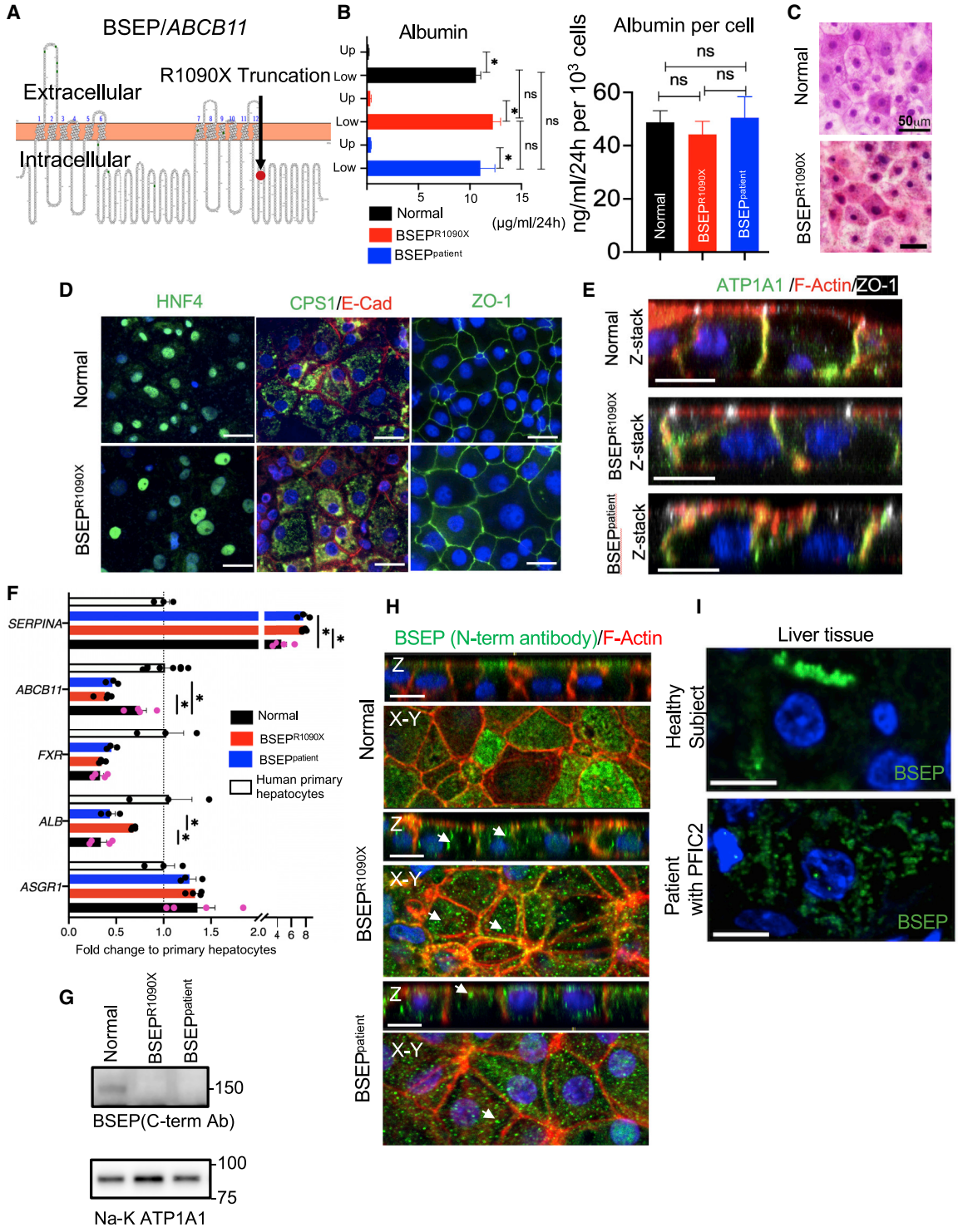

Figure 1. Hepatic differentiation of BSEP^{R1090X} and BSEP^{patient} iPSCs and BSEP protein expression

(A) Gene map of BSEP/*ABCB11* and location of the R1090X truncating mutation.

(B) (Left) Albumin concentration of the culture supernatant in the upper and lower chambers was measured with ELISA. The supernatant was collected 24 h after medium change. n = 6 independent differentiation experiments. (Right) Albumin secretion per i-Hep at the final stage of hepatic differentiation. At the final stage of hepatic differentiation, i-Heps were fixed and stained with Hoechst to measure the cellular (nuclear) density by counting nuclei under the fluorescent microscope. All i-Heps exhibited comparable albumin secretion into the

(legend continued on next page)

on the lateral membrane, while the basal membrane was not depicted by our confocal microscope settings due to the optical interference of the Transwell membrane. ZO1 was detected at the corner of the cells where apical and lateral membranes meet. These results indicate intact cellular polarity in normal cells, BSEP^{R1090X} i-Heps, and BSEP^{patient} i-Heps. To further compare the hepatocellular differentiation among the i-Heps, gene expression levels of hepatic markers were compared by quantitative PCR. Hepatocyte markers (*FXR*, *ASGR1*) were comparable among i-Heps. BSEP^{R1090X} and BSEP^{patient} i-Heps expressed more *SERPINA1*/α1 antitrypsin, another hepatocyte marker, compared with normal i-Heps. *ALB*/albumin was expressed most in BSEP^{R1090X}. The gene expression of *ABCB11*/BSEP was less in BSEP^{R1090X} and BSEP^{patient} i-Heps, compared with normal i-Heps (Figure 1F). The gene expression from primary cultured human hepatocytes was used as a reference.

Next, to determine whether genomic editing of the *ABCB11* gene alters the BSEP protein expression pattern, we performed western blotting and immunofluorescent staining of BSEP. An antibody targeting the C terminus of the protein detected BSEP in normal i-Heps but did not detect BSEP in BSEP^{R1090X} and BSEP^{patient} i-Heps (Figure 1G). Immunostaining with another antibody targeting the N terminus revealed that the BSEP^{R1090X} and BSEP^{patient} i-Heps expressed BSEP protein in an aberrant pattern (Figure 1H). Whereas normal i-Heps expressed BSEP mainly at the apical membrane of monolayer cells, BSEP was localized in the cytosol in a dot-like pattern in BSEP^{R1090X} and BSEP^{patient} i-Heps. F-actin was also stained to localize the apical and lateral membrane. To determine whether the apical membrane of BSEP^{R1090X} i-Heps maintains other transporters, we stained i-Heps with antibodies against MDR1 (Figure S2E). In both normal and BSEP^{R1090X} i-Heps, MDR1 localized to the apical membrane. To determine whether the pattern of BSEP expression reflects the cellular localization in liver tissue of patients with PFIC2, we performed immunofluorescent staining of liver biopsy specimens using the same N-terminal antibody (Figure 1I). Compared with hepatocytes obtained from the liver of a healthy subject, where BSEP is localized at a canalicular membrane structure, BSEP in hepatocytes of the patients with PFIC2 was localized in the cytosol in a clustering pattern. These results indicate that genomic editing of the *ABCB11* gene in iPSCs results in the aberrant localization of BSEP in i-Heps, comparable to the pattern of BSEP localization seen in the hepatocytes of the liver of the patient with PFIC2.

Cellular Ultrastructure in BSEP^{R1090X} i-Heps Recapitulates Hepatocyte Abnormalities in the Liver Tissue of the Patient with PFIC2

It has been reported that the development of microvilli on the bile canaliculus depends on the export of bile acid across the canalicular membrane of hepatocytes (Bove et al., 2004). To investigate the effect of the altered BSEP expression pattern, we performed a morphological analysis of i-Heps derived from normal and BSEP^{R1090X} iPSCs. To assess ultrastructural changes, i-Heps at the last stage of

culture medium. See Figure S2A for cell counts of i-Heps (ns, not significant; *p < 0.05, n = 5 or more independent differentiation experiments).

(C) Conventional light microscopic images of H&E staining of normal and BSEP^{R1090X} i-Heps. Scale bar: 50 μm.

(D) Immunofluorescent staining of normal and BSEP^{R1090X} i-Heps at the final stage of the differentiation protocol. Hepatocyte markers, HNF4a and CPS1, were detected in both normal and BSEP^{R1090X} (green) cells. An endoderm marker of E-cadherin was detected on the cell membrane (red). A tight-junction protein, ZO1, was located at the borders of cells (green). Nuclei were stained with Hoechst (blue). See also Figure S2C for BSEP^{patient} i-Heps. Scale bar: 10 μm.

(E) Confocal microscopic images of immunofluorescent staining for i-Heps with z-stack reconstruction. In all i-Heps, the basolateral marker, ATP1A1 (green), was detected on the lateral membrane. The polarity marker, F-actin (red), was detected mainly on the apical membrane in all i-Heps with some overlap with the lateral membrane. A tight-junction protein, ZO1, was located at the corners of the cells (white). Nuclei were stained with Hoechst (blue). Scale bar: 10 μm.

(F) Gene expression of hepatic differentiation markers in i-Heps. Marker genes of hepatocyte differentiation were compared by quantitative PCR after normalization to 18S rRNA. At the final stage of differentiation, total RNA was extracted from i-Heps. RNA extracts from primary cultured human hepatocytes were used as control and reference for relative expression of hepatic genes (no marks, ns; *p < 0.05; n = 3 or 4 independent experiments, pink and black dots represent average values of fold change from each experiment; the comparison with primary hepatocytes was not displayed). 18S rRNA housekeeping gene expression did not differ between cell types (p > 0.05).

(G) Western blotting to detect proteins of BSEP from cell lysates of i-Heps by using antibody detecting the C terminus of BSEP. BSEP^{R1090X} and BSEP^{patient} i-Heps showed no band compared with the normal i-Hep lysate. Na-K ATPase (ATP1A1) was included as a loading control.

(H) Confocal images and z-stack reconstruction images of immunofluorescent staining of i-Heps using the antibody targeting the N terminus of BSEP. BSEP (green), F-actin (red), and nuclei (blue) were detected. BSEP is localized on the apical membrane of normal i-Heps and in the cytosol of BSEP^{R1090X} and BSEP^{patient} i-Heps (arrows). F-actin is expressed on the apical and lateral membrane. Scale bar: 10 μm.

(I) Immunofluorescent images of liver tissue in paraffin sections from a healthy subject and the patient with BSEP^{R1090X} truncating mutation. BSEP is localized at the canalicular membrane structure in the hepatocytes of a healthy subject. The protein with BSEP^{R1090X} mutation is localized in the cytosol, with a clustering pattern, in the hepatocytes of the patient with PFIC2. Scale bar: 10 μm.

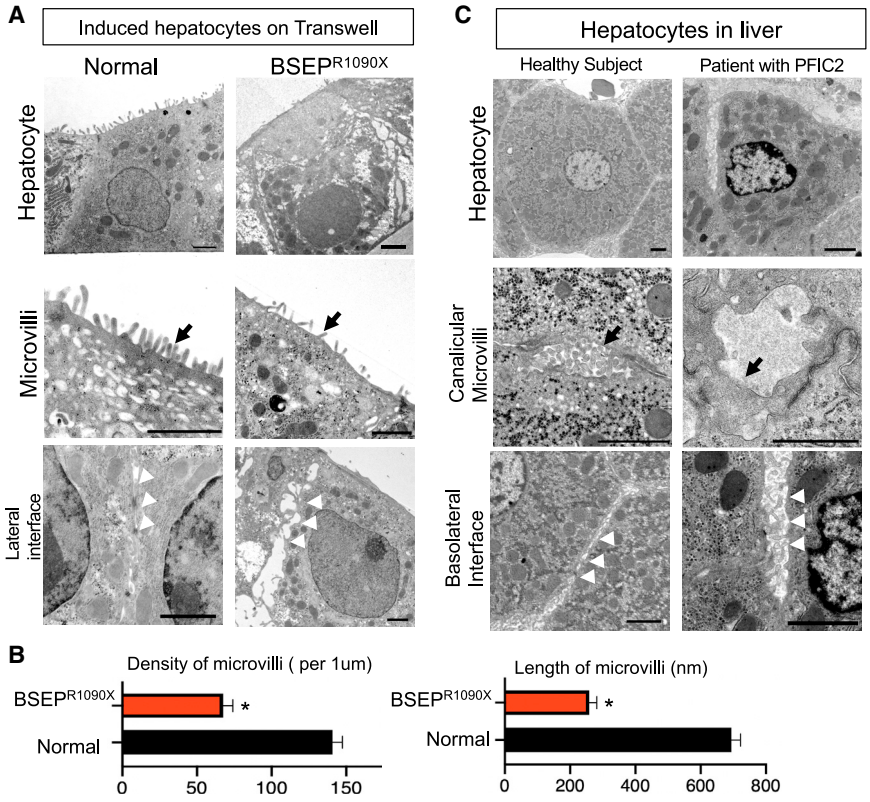

Figure 2. Cellular ultrastructure of BSEP^{R1090X} i-Heps recapitulates the abnormalities observed in the liver tissue of the patient with PFIC2

(A) Electron microscopic (EM) images of normal (left column) and BSEP^{R1090X} i-Heps (right column). Cells on the Transwell membrane were cross sectioned. Normal i-Heps showed dense microvilli on the apical surface, whereas BSEP^{R1090X} i-Heps showed sparse microvilli (black arrows). Basolateral membrane irregularity with wider interstitial space between hepatocytes was observed in BSEP^{R1090X} (white arrowheads).

(B) Morphometric analysis of microvilli in the EM images. The density of apical microvilli was counted per cell (left). The length of the microvilli was measured by morphometric tools in ImageJ software and averaged per cell (right). *$p < 0.05$, $n = 30$ cells per i-Hep genotype, three independent differentiation experiments.

(C) EM images of liver tissues from a healthy subject (left column) and the patient with PFIC2 (right column). The hepatocytes of the patient's liver showed decreased microvilli in the bile canaliculus (black arrows) and wider interstitial space between the basolateral membranes of adjacent cells (white arrowheads). Scale bar: 2 μm.

differentiation were evaluated by electron microscopy (Figure 2A). Normal i-Heps showed a monolayer structure with dense microvilli on the apical membrane. These findings indicate that i-Heps developed epithelial polarization as a monolayer on the Transwell membrane, directing the apical membrane toward the upper chamber and the basal interface toward the lower chamber via the permeable membrane of the Transwell. BSEP^{R1090X} showed fewer and shorter microvilli on their apical surface, indicating reduced bile acid transport across the apical membrane (Figure 2B). We also found irregularity of the basolateral membrane in BSEP^{R1090X}, with wider interstitial space between hepatocytes. To determine whether these ultrastructural features are relevant to the patient with PFIC2 (R1090X mutation), the liver explant obtained at the time of liver transplant was investigated via electron microscopy (Figure 2C). Compared with hepatocytes from a normal liver, hepatocytes from the patients with PFIC2 exhibited a decreased number of microvilli in the bile canaliculus and wider interstitial space between basolateral membranes of adjacent cells. These corresponding morphological features between i-Hep and liver suggest that the pathological process of the patient with the truncating mutation manifests in BSEP^{R1090X} i-Heps.

BSEP^{R1090X} Is Deficient in Exogenous Bile Acid Transport via the Basolateral-to-apical Phase

The structural defect of microvilli on the apical surface on BSEP^{R1090X} i-Heps suggested compromised canalicular function, specifically in bile acid export. To examine how the BSEP truncation affects the exporting function of BSEP in response to exogenous bile acids, we next evaluated the capability of bile acid transport of i-Heps by adding TCA to the lower chamber. In our previous study, we demonstrated that normal i-Heps transport bile acids from the basolateral to the apical phase (transcellular transport from sinusoid to bile canaliculus) (Asai et al., 2017). To assess whether BSEP^{R1090X} and BSEP^{patient} i-Heps manifest altered transcellular transport of conjugated bile acids, we first measured the amount of TCA in culture medium from the upper chamber 24 and 48 h after loading TCA in the lower chamber. In normal i-Heps, the amount of transported TCA in the upper chamber increased at 24 h, with the majority of the loaded TCA traversing from the lower to the upper chamber by 48 h. In contrast, in BSEP^{R1090X} and BSEP^{patient} i-Heps, most of the loaded TCA remained in the lower chamber (Figures 3A–3C and S3). These data formed the first indication that the transport direction of conjugated bile acids in BSEP^{R1090X} and

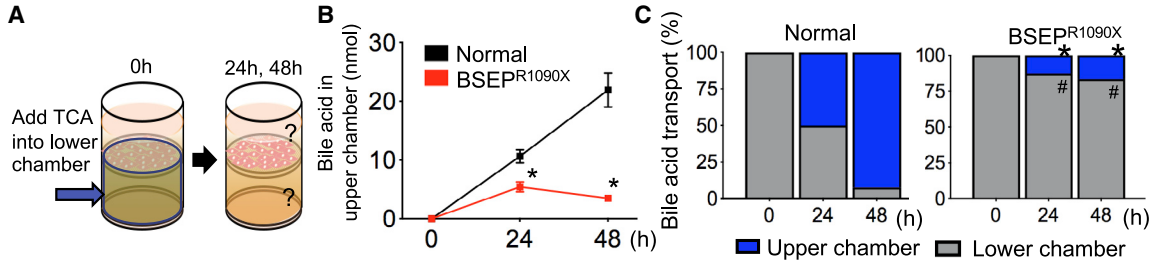

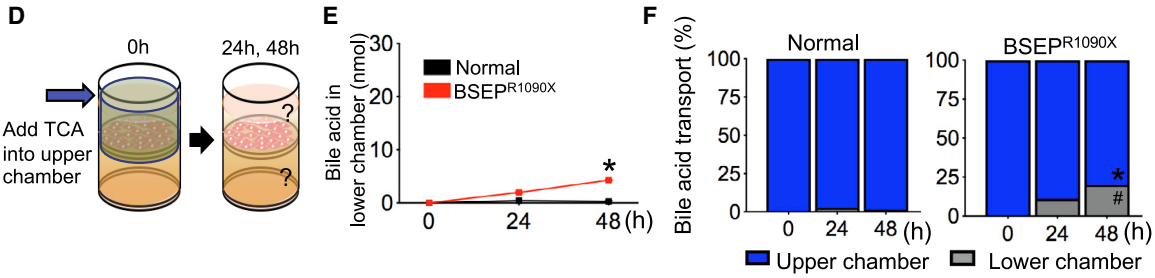

G

Permeability (% of the probe leaked into the opposite chamber)

Direction	Normal	BSEP R1090X	P value
Lower to Upper	1.2 +/- 0.23 %	1.1 +/- 0.19 %	0.58
Upper to Lower	0.9 +/- 0.16 %	0.7 +/- 0.12 %	0.42

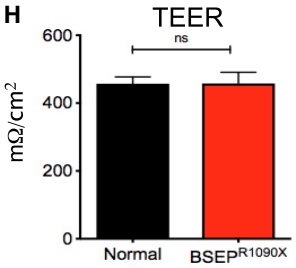

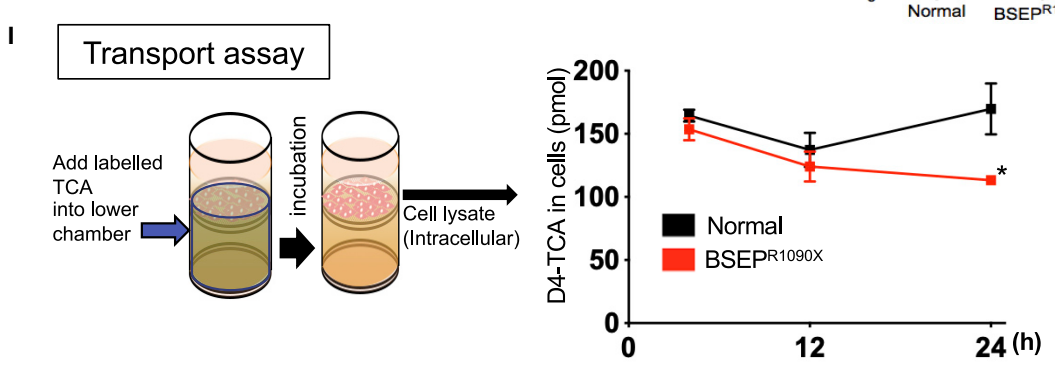

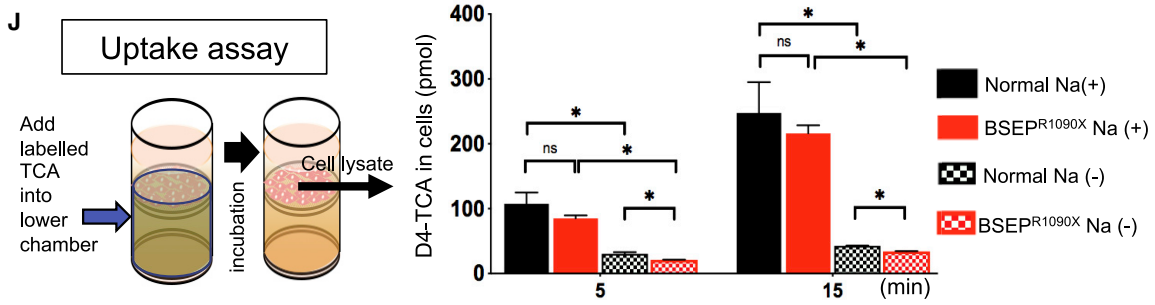

(legend on next page)

BSEP^{patient} i-Heps differs from the direction seen in normal i-Heps. To determine whether this direction of exogenous TCA transport is specific to a basolateral-to-apical direction, we measured the amount of TCA in the lower chamber after loading it into the upper chamber (Figures 3D–3F). In both normal and BSEP^{R1090X}, most of the loaded TCA remained in the upper chamber. To measure the degree of paracellular "leak" of TCA, we compared the permeability of the monolayers in normal and BSEP^{R1090X} i-Heps (Figure 3G). After 48 h, a minimal, comparable amount of the fluorescent probe (10,000 MW dextrose-conjugated Alexa Fluor) was transported from the lower to the upper chamber in both normal and BSEP^{R1090X}. Furthermore, to compare their barrier function as monolayers, we measured *trans*-epithelial electrical resistance between the upper and the lower chamber (Figure 3H). Cellular viability was comparable between i-Heps (Figure S3B). The resistance of the BSEP^{R1090X} monolayer was comparable to that of the normal i-Hep monolayer. Together, these results demonstrate that BSEP^{R1090X} i-Heps exhibit a specific deficiency in basolateral-to-apical transcellular transport of conjugated bile acids.

Intracellular TCA in BSEP^{R1090X} i-Heps Remains Comparable to that of Normal i-Heps during Transcellular Transport of TCA

To test whether decreased bile acid export induces intracellular accumulation of TCA in BSEP^{R1090X}, we performed molecular tracing experiments and quantified TCA concentration in cell lysates after loading TCA into the lower chamber. By using isotope-labeled TCA (D4-TCA), we measured the export and uptake of TCA executed by i-Heps independent of endogenous TCA. First, we determined whether BSEP^{R1090X} i-Heps accumulate more intracellular TCA than normal i-Heps when exposed to exogenous TCA from the lower chambers (Figure 3I). To quantify the long-term transport activity, we performed a 24-h tracing experiment. After loading D4-TCA in the lower chambers (1 μM), we quantified the amount of D4-TCA in the cell lysates at 4, 12, and 24 h. At each time point in BSEP^{R1090X} i-Heps, the cell lysates contained comparable (4 and 12 h) or smaller amounts (24 h) of D4-TCA compared with the normal i-Heps. This result demonstrates that BSEP^{R1090X} i-Heps do not accumulate intracellular TCA to a greater degree than the normal i-Heps, despite having decreased apical export of TCA.

The result prompted us to test whether BSEP^{R1090X} i-Heps have a comparable capability to take up D4-TCA from the lower chamber by measuring intracellular D4-TCA after a short period of time before their saturation was reached. At a physiological dose of TCA (10 μM) in the culture medium in the lower chamber, normal and BSEP^{R1090X} i-Heps showed comparable amounts of uptake at 5 and 15 min of incubation time (Figure 3J). To test whether D4-TCA uptake was sodium dependent, we measured intracellular D4-TCA after incubation with sodium-depleted culture medium. In both normal and BSEP^{R1090X} i-Heps, the intracellular D4-TCA was significantly lower compared

Figure 3. Dynamics of the basolateral-to-apical transport of TCA in BSEP^{R1090X} i-Heps

(A) Experimental scheme of exogenous TCA transport from the lower chamber to the upper chamber.

(B) The amount of bile acid in the upper chamber was measured at 24 and 48 h after loading TCA in the lower chamber. *p < 0.05, n = 5 independent differentiation experiments.

(C) Percentages of the sum of bile acids measured from the upper and lower chambers in a well at 0, 24, and 48 h after loading of TCA. Gray: percentage of bile acids measured in the lower chamber. Blue: in the upper chamber. *p < 0.05, mean of the upper chamber, normal versus BSEP^{R1090X}; #p < 0.05, mean of the lower chamber, normal versus BSEP^{R1090X}; n = 5 independent differentiation experiments.

(D) Experimental scheme of TCA transport from the upper chamber to the lower chamber.

(E) The mass of bile acid in the culture medium in the lower chamber, 24 and 48 h after loading TCA in the upper chamber. *p < 0.05, n = 5 independent differentiation experiments.

(F) Percentage of measured bile acid in a well at 0, 24, and 48 h after loading of TCA. Gray: percentage of bile acids measured in the lower chamber. Blue: in the upper chamber. *p < 0.05, mean of the upper chamber, normal versus BSEP^{R1090X}; #p < 0.05, mean of the lower chamber, normal versus BSEP^{R1090X}; n = 5 independent differentiation experiments.

(G) Permeability of the monolayer between the upper and the lower chambers measured with dextrose-conjugated fluorescent probe (10,000 MW Alexa Fluor). The probe was measured in the culture supernatant in the chambers 48 h after loading into the opposite chambers, described as a percentage (±SD) of the initial amount of loaded probe. n = 3 independent experiments.

(H) Monolayer barrier function is measured with *trans*-epithelial electrical resistance (TEER) between the upper and the lower chambers via monolayer and Transwell membrane. ns, not significant, p > 0.05, n = 5 independent experiments.

(I) Transport assay of isotope-labeled TCA (D4-TCA) to determine the intracellular accumulation of TCA over a 24-h period. D4-TCA (1 μM) was added into the lower chamber. The amount of TCA was quantified by mass spectrometry in the cell lysates collected at 4, 12, and 24 h after loading. The amount of D4-TCA was calculated per well. *p < 0.05, n = 3 independent experiments.

(J) Uptake assay of D4-TCA. D4-TCA (10 μM) was added into the lower chamber and cell lysates were collected after 5 and 15 min incubation with or without sodium in the culture medium. Without sodium in the culture medium, D4-TCA was not taken up by the i-Heps. ns, not significant; *p < 0.05, n = 3 independent experiments.

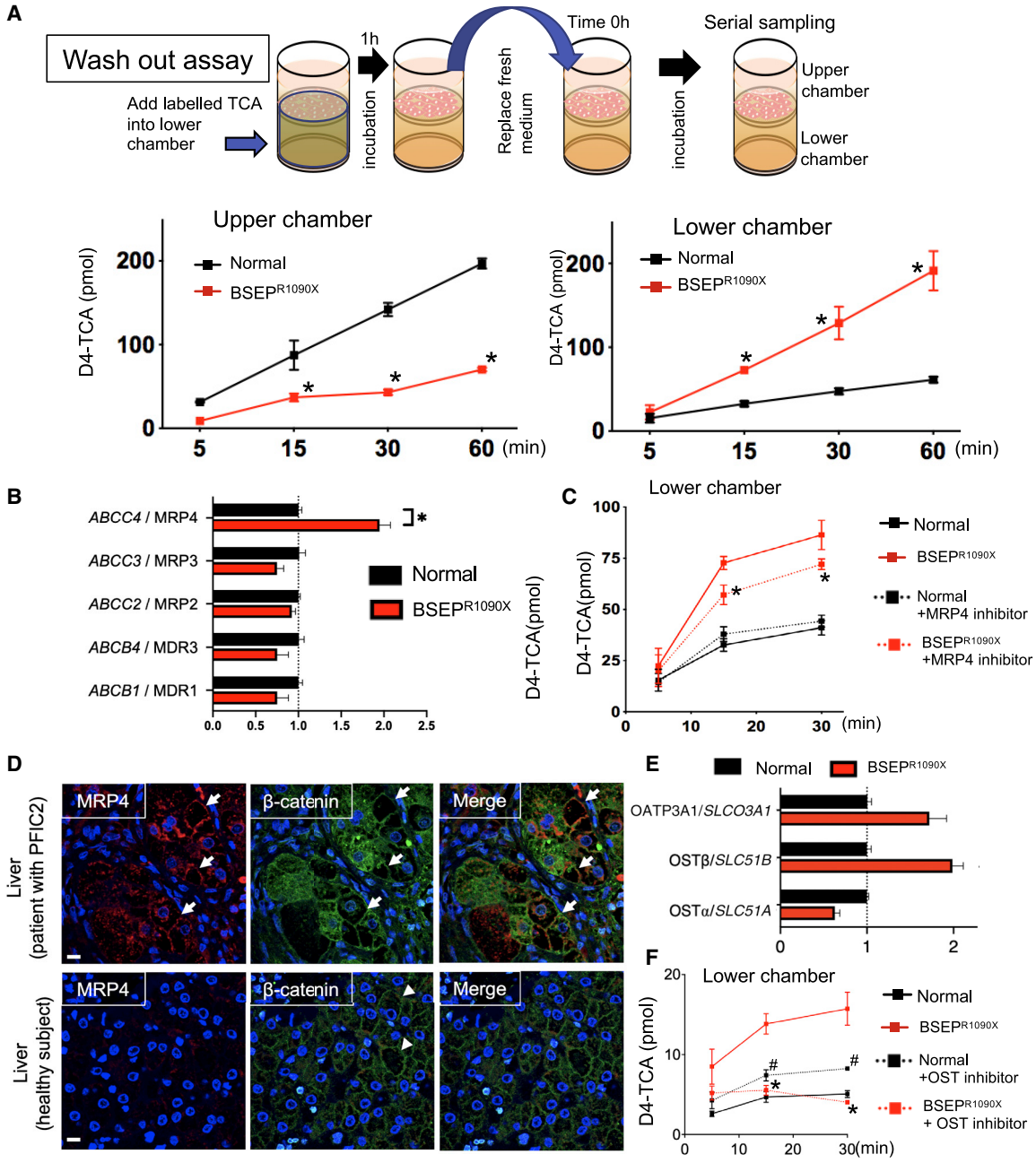

Figure 4. BSEP^{R1090X} i-Heps export intracellular TCA back into the lower chambers via basolateral MRP4 and OST

(A) Washout assay to determine the transport (efflux) direction of intracellular D4-TCA. After 1 h of D4-TCA incubation in the lower chamber (10 μM), i-Heps were washed with medium and placed in a fresh medium. The intracellular D4-TCA was exported into the fresh medium in the upper and lower chambers and measured at 5, 15, 30, and 60 min by mass spectrometry. BSEP^{R1090X} i-Heps showed basolateral excretion of TCA as opposed to normal i-Heps, which excrete TCA apically. *$p < 0.05$, $n = 3$ independent experiments.

(B) Gene expression of hepatic ABC transporters in i-Heps at the final stage of differentiation was measured by quantitative real-time PCR ($n = 4$ independent experiments). After normalization to 18S rRNA, each gene expression level was shown relative to the expression level in normal i-Heps. Compared with normal i-Heps (*$p < 0.05$), the BSEP^{R1090X} i-Heps expressed more *ABCC4*/MRP4. 18S rRNA housekeeping gene expression did not differ between cell types ($p > 0.05$).

(C) Washout assay to determine the role of MRP4 in intracellular-to-basolateral export of D4-TCA by using an MRP4 inhibitor (Ceefourin 1). After 1 h of D4-TCA incubation in the lower chamber (10 μM), i-Heps were washed and placed in a fresh medium with or without MRP4

(legend continued on next page)

with that in the condition of sodium-containing regular culture medium. Cellular viability was comparable among conditions of i-Heps (Figures S3C and S3D). These results indicate that BSEP^{R1090X} i-Heps exhibit comparable capability of TCA uptake in a sodium-dependent fashion. Together, the accumulation of intracellular TCA in BSEP^{R1090X} i-Heps was comparable to that in normal i-Heps in the setting where they take up comparable amounts of the conjugated bile acid across the basolateral surface into the intracellular space, while having deficient export of TCA across the apical membrane.

BSEP^{R1090X} i-Heps Export Intracellular TCA via the Basolateral Membrane toward the Lower Chamber

Because BSEP^{R1090X} i-Heps have a limited capacity for the apical export of TCA while taking up comparable amounts of TCA, these results suggested that BSEP^{R1090X} compensates via other export channels, potentially basolateral export. To determine whether BSEP^{R1090X} i-Heps export intracellular TCA via the basolateral membrane after uptake of TCA, we performed a "washout" tracing experiment with D4-TCA. After 1 h of incubation for the uptake of D4-TCA from the lower chamber, i-Heps were washed gently with medium and incubated in a fresh culture medium. At 5, 15, 30, and 60 min, we quantified D4-TCA in the upper and lower chamber to determine the export rates from the apical and basolateral membranes, respectively (Figure 4A). The BSEP^{R1090X} i-Heps showed increased export into the lower chamber compared with normal i-Heps at each time point. In addition, BSEP^{R1090X} showed greater export toward the lower chamber than toward the upper chamber, as seen at later time points. The normal i-Heps showed the opposite export pattern compared with BSEP^{R1090X} i-Heps. These results indicate that BSEP^{R1090X} i-Heps utilize basolateral export of intracellular TCA when their apical export is deficient. To identify transporters on the basolateral membrane of BSEP^{R1090X} i-Heps, we profiled the gene expression of the transmembrane ATP binding cassette (ABC) transporters by quantitative RT-PCR. We found a gene upregulation of *ABCC4*/MRP4, known to transport conjugated bile acids, including TCA (Figure 4B). To further determine the functional role of MRP4 in the basolateral export of BSEP^{R1090X} i-Heps, we performed washout tracing experiments with and without the MRP4 inhibitor (Ceefourin 1) in the culture medium (Cheung et al., 2014). Ceefourin 1 decreased the basolateral export of TCA in BSEP^{R1090X} i-Heps, while it did not alter the basolateral export in the normal i-Heps (Figure 4C). Cellular viability was comparable between i-Heps (Figures S3E and S3F). To determine whether hepatocytes in the patient with PFIC2 expressed MRP4 on the basolateral membrane, we performed immunofluorescent staining on the liver paraffin sections. MRP4/*ABCC4* was detected on the plasma membrane of hepatocytes from the patient with PFIC2; this co-localized with β-catenin, indicating that MRP4 is expressed on the basolateral membrane (Figure 4D). MRP4 was not detected on the plasma membrane of hepatocytes from the healthy subject. These results indicate that MRP4 plays a role in the intracellular-to-basolateral export of TCA in BSEP deficiency. Because MRP4 showed a partial role in the basolateral export in BSEP^{R1090X} i-Heps, we explored the possible contribution of other transporters that are capable of carrying bile acids. Among the SLC family, OSTα/*SLC51A*, OSTβ/*SLC51B*, OATP3A1/*SLCO3A1*, and OATP1B3/*SLCO1B3* are known to export conjugated bile acid from the basolateral domain (Alrefai and Gill, 2007; Ballatori et al., 2009; Briz et al., 2006; Bruyn et al., 2011; Pan et al., 2018). We found gene upregulation of OSTβ/*SLC51B* and OATP3A1/*SLCO3A1* in BSEP^{R1090X} i-Heps and downregulation of OSTα/*SLC51A* (Figure 4E). Of note, OSTα and OSTβ form a complex on the basolateral membrane. Both subunits are required to function; however, OSTβ plays a regulatory role in the transport function (Ballatori et al., 2013; Christian et al., 2012). The gene expression of OATP1B3/*SLCO1B3* was negligible in both i-Heps. To evaluate the role of OST in

inhibitor. The exported D4-TCA in the lower chamber was measured by mass spectrometry at 5, 15, and 30 min. At 15 and 30 min, MRP4 inhibitor decreased D4-TCA export toward the lower chamber. *$p < 0.05$, $n = 4$ independent experiments.

(D) Human liver paraffin sections were co-stained with anti-MRP4 and anti-β-catenin antibodies and visualized with immunofluorescent secondary antibodies. MRP4/*ABCC4* was detected on the plasma membrane of hepatocytes from the patient with PFIC2 and co-localized with β-catenin (white arrows). MRP4 was not detected in hepatocytes from the healthy subject, but β-catenin was detected on the plasma membrane (white arrowheads). Scale bar: 1 μm.

(E) Gene expression of SLC transporters in i-Heps at the final stage of differentiation was measured by quantitative real-time PCR ($n = 4$ independent experiments). After normalization to 18S rRNA, each gene expression level was shown relative to the expression level in normal i-Heps. Compared with normal i-Heps (*$p < 0.05$), the BSEP^{R1090X} i-Heps expressed more *SLC51B* and *SLC03A1* and less *SLC51A*. 18S rRNA housekeeping gene expression did not differ between cell types ($p > 0.05$).

(F) Washout assay to determine the role of OST in intracellular-to-basolateral export of D4-TCA by using an inhibitor of OST (clofazimine, 30 μM). After 1 h of D4-TCA incubation in the lower chamber (10 μM), i-Heps were washed and placed in a fresh medium with or without an OST inhibitor. The exported D4-TCA in the lower chamber was measured by mass spectrometry at 5, 15, and 30 min and displayed. At 15 and 30 min, the OST inhibitor decreased D4-TCA export toward the lower chamber. BSEP^{R1090X}, no treatment versus OST inhibitor, *$p < 0.05$, $n = 4$ independent experiments. Normal, no treatment versus OST inhibitor, #$p < 0.05$, $n = 4$ independent experiments.

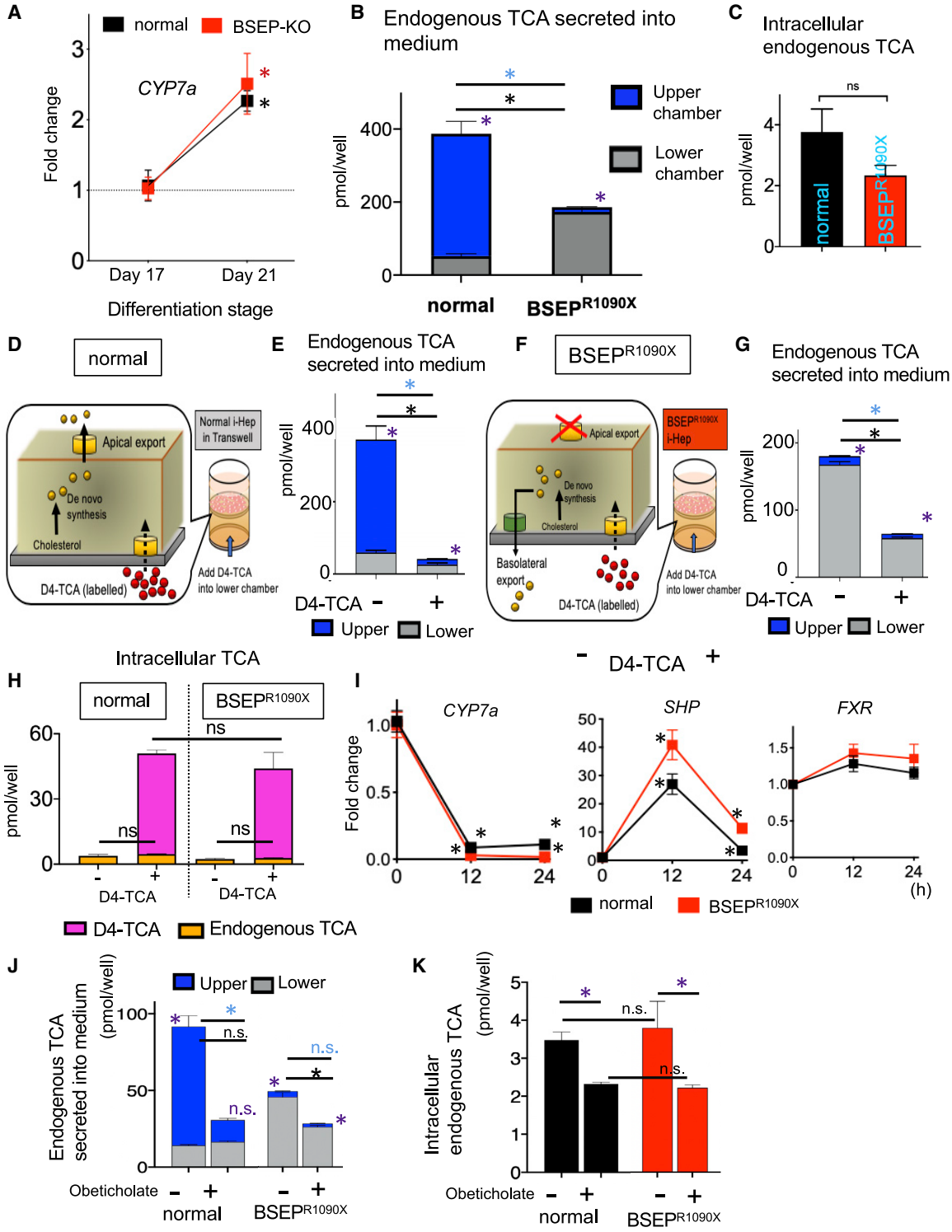

Figure 5. BSEP^{R1090X} i-Heps adapt export of synthesized bile acids via the basolateral membrane and respond to exogenous bile acids

(A) Gene expression of *CYP7a* in i-Heps is measured by RT-PCR at the last stages of differentiation. In both normal and BSEP^{R1090X} i-Heps, *CYP7a* expression increased from day 17 of culture to day 21. The fold change in gene expression was based to the values of day 17. *p < 0.05, day 17 versus day 21, n = 3 independent experiments.

(legend continued on next page)

the basolateral export, we quantified D4-TCA export into the lower chamber with and without the OST inhibitor clofazimine (Malinen et al., 2018). When OST was inhibited, the basolateral export of D4-TCA was reduced (Figure 4F), indicating that OST plays a role in the basolateral export of TCA. We also tested if OATP3A1/*SLCO3A1* plays a role in TCA export by using the same methods; however, we did not detect a role for OATP3A1 in the basolateral export in our model system (Figure S3H). These results suggest that a combination of basolateral transporters play a role in exporting intracellular bile acids in BSEP^{R1090X} i-Heps. Together, during exposure to exogenous TCA, our results demonstrate that BSEP^{R1090X} i-Heps maintain low intracellular TCA concentration by export via basolateral membrane transporters.

BSEP^{R1090X} i-Heps Adapt an Alternative Export of Newly Synthesized Bile Acids via the Basolateral Membrane

Cholestasis in patients with PFIC2 becomes prominent during the first few weeks after birth as hepatocytes initiate *de novo* bile acid synthesis. Based on the findings of basolateral export of exogenous bile acids, we investigated the fate of intracellular endogenous bile acids synthesized in BSEP-deficient hepatocytes. To determine in which stage the i-Hep culture system induces *de novo* bile acid synthesis, we measured changes in gene expression of *CYP7a*, a master regulator of bile acid synthesis in hepatocytes, by RT-PCR. Both normal and BSEP^{R1090X} i-Heps exhibit minimal expression of *CYP7a* until day 17 of the differentiation stage; then, at the final stage of the differentiation (day 21), *CYP7a* expression is increased in both normal and BSEP^{R1090X} i-Heps (Figure 5A). This suggests that i-Heps start synthesizing bile acids *de novo* at the last stage of the differentiation process. To assess the impact of truncated BSEP on the export of intracellular bile acids synthesized *de novo*, we measured the concentration of endogenous TCA secreted into the culture medium from i-Heps (Figure 5B). After 48 h of incubation in a fresh culture medium, we collected the culture supernatant from the upper chamber and lower chamber separately, as well as the cell lysates. The normal i-Heps exported more TCA into the upper chamber than into the lower chamber. This suggests that normal i-Heps predominantly export TCA via the apical membrane. Consistent with abnormal BSEP function, BSEP^{R1090X} i-Heps exported a diminished amount of TCA into the upper chamber but significantly more TCA into the lower chamber, indicating that BSEP^{R1090X} i-Heps

(B) The amount of endogenous taurocholic acid (TCA) exported into the upper chamber (blue) and lower chamber (gray) was measured by mass spectrometry. After incubation in a fresh culture medium for 48 h, the TCA concentrations in the culture supernatant from the upper and lower chambers were determined. Normal i-Heps exported endogenous TCA toward the upper chamber (apical domain) and BSEP^{R1090X} i-Heps toward the lower chamber (basolateral domain). The total amount of TCA synthesized by BSEP^{R1090X} i-Heps was less than that by normal i-Heps. *$p < 0.05$: black, lower chamber normal versus BSEP^{R1090X}; blue, upper chamber normal versus BSEP^{R1090X}; purple, upper chamber versus lower chamber of each i-Hep, n = 3 independent experiments.

(C) The amount of intracellular TCA was measured from cell lysates after 48 h of incubation. Intracellular TCA amounts in normal and BSEP^{R1090X} i-Heps were comparable. ns: $p > 0.05$, n = 3 independent experiments.

(D) Schematic description of experiment design in normal i-Heps. Labeled TCA, D4-TCA, was added to the lower chamber. After the incubation, TCA (endogenous and D4-TCA) in the culture medium was measured separately.

(E) The amount of endogenous TCA secreted into the upper and lower chambers was measured under the conditions cultured with or without exogenous D4-TCA. The exogenous D4-TCA suppressed endogenous synthesis of TCA. *$p < 0.05$: black, lower chambers cultured with versus without D4-TCA; blue, upper chambers cultured with versus without D4-TCA; purple, upper chamber versus lower chamber of each i-Hep, n = 3 independent experiments.

(F) Schematic description of experiment design in BSEP^{R1090X} i-Heps.

(G) The amount of endogenous TCA secreted into the upper and lower chambers was measured under the conditions cultured with or without exogenous D4-TCA. *$p < 0.05$: black, lower chambers cultured with versus without D4-TCA; blue, upper chambers cultured with versus without D4-TCA; purple, upper chamber versus lower chamber of each i-Hep, n = 3 independent experiments.

(H) Intracellular TCA, endogenous and D4-TCA, measured separately from the cell lysate after the incubation. Exogenous D4-TCA amounts accumulated in normal and BSEP^{R1090X} i-Heps are comparable. ns: $p > 0.05$, n = 3 independent experiments.

(I) Gene expression of the FXR pathway was determined by RT-PCR. In both normal and BSEP^{R1090X} i-Heps, *CYP7a* was downregulated and *SHP* was upregulated when D4-TCA was added into the lower chamber for 12 and 24 h. No significant change was found in *FXR* expression. The fold change in gene expression was based on the values in the condition cultured without D4-TCA. *$p < 0.05$, n = 3 independent experiments.

(J) The amount of endogenous TCA secreted into the upper and lower chambers was measured under the conditions with or without FXR agonist obeticholic acid (OCA, 10 μM) in normal and BSEP^{R1090X} i-Heps. OCA suppressed the endogenous synthesis of TCA. *$p < 0.05$, n = 4 independent experiments: black, lower chambers cultured with versus without OCA; blue, upper chambers cultured with versus without OCA; purple, upper chamber versus lower chamber of each i-Hep.

(K) Intracellular TCA, endogenous and D4-TCA, measured separately from the cell lysate after the incubation with versus without OCA. OCA suppressed intracellular TCA in normal and BSEP^{R1090X} i-Heps. *$p < 0.05$, n = 4 independent experiments.

predominantly export endogenous TCA via the basolateral membrane. To further determine whether BSEP^{R1090X} i-Heps accumulate endogenous TCA in the cytoplasm, we measured the intracellular amount of TCA in BSEP^{R1090X} and normal i-Heps (Figure 5C). BSEP^{R1090X} and normal i-Heps showed comparable amounts of intracellular TCA. To determine the specific role of BSEP in i-Heps, we also tested if inhibition of BSEP in normal i-Heps reproduces the phenotype of BSEP^{R1090X} i-Heps. When normal i-Heps were incubated with sitaxentan, a BSEP inhibitor (Kenna et al., 2015), the apical TCA export was reduced, while the basolateral export was unchanged, resembling the trend seen in BSEP^{R1090X} i-Heps (Figure S3I). These data indicate that hepatocytes with BSEP deficiency initiate bile acid export via the basolateral membrane when *de novo* bile acid synthesis commences, seemingly as an adaptive mechanism to prevent the accumulation of intracellular bile acids.

Basolateral Transport of Exogenous Bile Acids Suppresses the *De Novo* Synthesis of Endogenous Bile Acids via the FXR Pathway in BSEP^{R1090X} i-Heps

In normal hepatocytes, during transcellular transport of the sinusoidal bile acids to the bile canaliculus, *de novo* bile acid synthesis is suppressed. To determine whether sinusoidal bile acids in the basolateral domain suppress bile acid synthesis in BSEP-deficient hepatocytes, we simultaneously quantified *de novo* bile acid synthesis and transcellular bile acid transport using D4-TCA as an exogenous bile acid (Figures 5D and 5F). Exogenous D4-TCA (10 μM) was added to the lower chamber medium and was quantified by mass spectrometry, separately from the endogenous TCA. In normal i-Heps, while D4-TCA in the lower chamber was transported to the upper (data not shown), in the same time period, *de novo* synthesis of TCA by the normal i-Heps was significantly suppressed (Figure 5E). In contrast, D4-TCA was minimally transported to the upper chamber in BSEP^{R1090X} i-Heps (data not shown), but *de novo* synthesis of TCA was still significantly suppressed (Figure 5G). To determine changes in the intracellular TCA accumulation by exogenous D4-TCA, endogenous TCA and D4-TCA in the cell lysates after the incubation were measured (Figure 5H). Normal and BSEP^{R1090X} i-Heps accumulated comparable amounts of D4-TCA intracellularly. This result suggests that intracellular TCA, taken up by either normal or BSEP^{R1090X} i-Heps, regulates the rate-limiting step of bile acid synthesis. To determine whether the regulatory effect was mediated by the FXR pathway, we quantified gene expression of *FXR* and its target genes, *SHP* and *CYP7a*, in i-Heps after exogenous TCA was added to the lower chambers (Figure 5I). Both normal and BSEP^{R1090X} i-Heps exhibited FXR pathway activation, shown as an increased expression of *SHP* and decreased expression of *CYP7a* when importing TCA. Thus, we demonstrated that BSEP-deficient hepatocytes are able to suppress *de novo* bile acid synthesis via the FXR pathway when they are not transporting bile acids to the bile canaliculus. Recently, an FXR agonist, obeticholic acid, was approved by the FDA for the treatment of cholestatic liver diseases (Jones, 2016). To determine the effect of an FXR agonist on *de novo* bile acid synthesis of BSEP-deficient human hepatocytes, we quantified the endogenous TCA production of normal and BSEP^{R1090X} i-Heps when incubated with obeticholic acid. Similar to the exogenous TCA, obeticholic acid suppressed *de novo* synthesis of TCA in BSEP^{R1090X} i-Heps while reducing the intracellular accumulation of TCA (Figures 5J and 5K). This finding indicates that our BSEP-deficient model system is feasible for investigating the cellular mechanisms of bile acid transport and synthesis in human hepatocytes.

DISCUSSION

In this study, we provide new insight into the adaptive mechanism of cellular regulation of bile acid homeostasis in hepatocytes. We found that human hepatocytes with BSEP deficiency use basolateral transporters to export conjugated bile acids. Further, we found that BSEP-deficient hepatocytes regulate *de novo* bile acid synthesis via the FXR pathway when importing and exporting bile acids at the basolateral membrane, thereby maintaining the intracellular bile acid level.

Enterohepatic bile acid circulation reaches homeostasis by the interaction between transcellular bile acid transport and *de novo* synthesis mediated by intracellular bile acids in hepatocytes (Figure 6A). The BSEP-deficient hepatocytes export endogenous conjugated bile acids via the basolateral membrane as they synthesize bile acids. In patients with PFIC2, since sinusoidal bile acids are not transported into the enterohepatic circulation, they remain in the systemic circulation, leading to jaundice and cholestasis (Figure 6B). In this report, we demonstrated that BSEP-deficient hepatocytes are able to downregulate *de novo* bile acid synthesis via the uptake and export of bile acids on the basolateral domain while preventing the accumulation of intracellular bile acids. This suggests that *de novo* synthesis of bile acids can be suppressed in BSEP-deficient hepatocytes by exogenous bile acids. We demonstrated that the FDA-approved FXR agonist obeticholic acid has the potential to reduce *de novo* bile acid synthesis in BSEP-deficient hepatocytes. Our findings offer potential treatment options to reduce systemic circulating bile acids in patients with PFIC2 with an FXR activator in the early stage of life.

In line with our report, the upregulation of MRP4 protein has been reported in the liver of patients with PFIC2 (Keitel

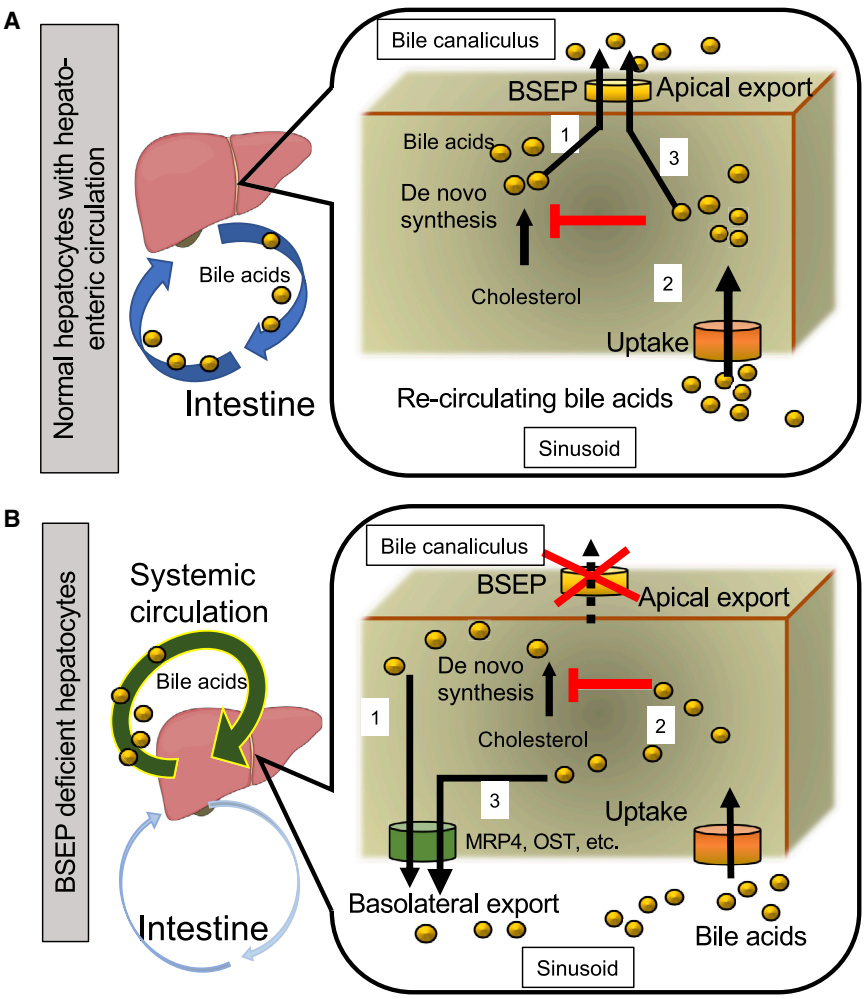

Figure 6. A model representing the mechanism regulating *de novo* bile acid synthesis in BSEP-deficient hepatocytes

(A) In normal hepatocytes, synthesized bile acids are exported to the bile canaliculus and return to the sinusoid by the hepatoenteric circulation (1). The bile acids in the sinusoid are taken up by hepatocytes and suppress *de novo* synthesis mediated by the intracellular concentration of bile acids (2 and 3).

(B) In BSEP-deficient hepatocytes, synthesized bile acids are exported to the sinusoid and accumulate in the systemic circulation (1). When taken up from the sinusoid, the intracellular bile acids suppress *de novo* bile acid synthesis while being exported to the sinusoid via the basolateral membrane (2 and 3).

et al., 2005). Our evidence of the role of MRP4 in basolateral bile acid export is compatible with the MRP4 expression on the basolateral membrane shown in their report. MRP4 has been reported to have a key role in cholestatic liver diseases (Mennone et al., 2006; Zollner et al., 2007). Similar to the previous reports, we found upregulation of other basolateral transporters (solute carrier organic anion transporters) in BSEP-deficient i-Heps. Based on our results, *SLC51*/OST is likely to be important in the adaptation. Together, it is feasible to suggest that human hepatocytes use basolateral MRP4 and OST, in part, to export intracellular bile acids into the sinusoid when canalicular export by BSEP is not possible.

Despite these compensatory responses to the BSEP deficiency, cellular injury and deformation in BSEP-deficient hepatocytes are prominent in the liver of PFIC2. The intracellular molecular mechanisms of hepatocyte injury due to BSEP deficiency remain unclear. A defect of MDR1 localization in BSEP-deficient zebrafish has been reported (Ellis et al., 2018). In our model system, human MDR1 was localized to the apical domain in BSEP-deficient i-Heps, suggesting a different regulation in human cells. It is possible that sinusoidal regurgitation of bile acids may trigger aberrant metabolic derangement of membrane phospholipids in the long term. It is also likely that paracrine excretion of bile acids into the sinusoidal space may induce an inflammatory response to the local innate immune cells, which may trigger a cytotoxic attack from the immune cells to the hepatocytes, resulting in cholestasis. Further investigation is under way to reveal this mechanism.

Our culture system induces hepatic differentiation into cells in a monolayer, where the apical membrane covers a wider surface area of the cells than the physiological bile canalicular structure of the hepatocytes. This condition limits the pharmacokinetic properties of BSEP function in i-Heps compared with that in hepatocytes *in vivo*. We used isogenic pairs of i-Heps to quantify the specific function of BSEP in hepatocytes; however, further advancement in bioengineering technology of microfluidics is required to overcome this limitation.

In summary, our findings reveal potentially novel mechanisms that underlie the pathophysiology of BSEP deficiency and may provide potential targets for therapeutic intervention in patients with PFIC2.

EXPERIMENTAL PROCEDURES

Human Specimens

The study protocol conformed to the ethical guidelines of the 1975 Declaration of Helsinki and was approved by the institutional review board of Cincinnati Children's Hospital Medical Center (ID: 2014-6705). Liver tissues from the subject were obtained from the explanted liver. Human primary hepatocytes in culture were purchased from GIBCO Fresh Hepatocytes service (Thermo Fisher, Waltham, MA) as described previously (Asai et al., 2017).

Cell Culture and Differentiation of iPSCs to Hepatocyte-like Cells

The iPSCs (clone: 1383D6) were derived from a healthy donor and provided by Kyoto University with a thorough characterization of pluripotency and karyotype (Takayama et al., 2017). For the reproduction of the study, we performed experiments on another iPSC clone (clone: TkDA3; kindly provided by K. Eto and H. Nakauchi). The results are summarized in Figures S4–S6. We generated iPSCs from the donated cells with the standard method of Yamanaka four-factor transfection. Protocols for endoderm differentiation, hepatic specification, and hepatocyte maturation were modified from previously described protocols and reported in the Supplemental Methods (Asai et al., 2017).

Measurement of Bile Acid Concentration in Culture Medium

Stable isotope-labeled TCA (sodium TCA, [2,2,4,4-$^{2}H_4$]TCA, here referred to as D4-TCA) was purchased from Cambridge Isotope Laboratories (Tewksbury, MA). The detailed methods of the tracer experiments and liquid chromatography-mass spectrometry are described in the Supplemental Methods.

Statistics

All *in vitro* experiments were performed at least in triplicate. Experimental values are expressed as the mean ± SEM, and statistical significance was determined by two-tailed Student's t test or by two-way ANOVA for comparison between three or more groups, followed by Bonferroni's multiple comparison *post hoc* tests with a significance set at $p < 0.05$.

SUPPLEMENTAL INFORMATION

Supplemental Information can be found online at https://doi.org/10.1016/j.stemcr.2020.12.008.

AUTHOR CONTRIBUTIONS

H.H., E.A., M.S., and A.A. designed and performed experiments, analyzed the data, and wrote the manuscript; S.O., K.S., A.F., E.K., Y.S., A.M., N.N., and W.Z. performed experiments and analyzed the data; H.K., S.H., T.N., Y.H., C.M., K.S., and T.T. contributed to experimental design and interpretation of the data and wrote the manuscript.

CONFLICTS OF INTEREST

A.A. and H.H. are listed as inventors on a patent related to this study, International Publication No. WO 2020/097555. K.S. holds equity in Asklepion Pharmaceuticals LLC and Aliveris s.r.l. and is a consultant to Retrophin.

ACKNOWLEDGMENTS

We thank Drs. William Balistreri, Jorge A. Bezerra, and James Wells for their advice in scientific discussion and manuscript preparation. We thank Sanjay Subramanian for his work in immunohistochemistry experiments. We also thank Drs. K. Eto, M. Otsu, and H. Nakauchi at Tokyo University and Dr. Yamanaka at CiRA for providing iPSCs. This work was supported by NIH grant P30 DK078392, a Pilot & Feasibility Award, the AASLD Foundation (Pinnacle Research Award), the NASPGHAN Foundation (George Ferry Young Investigator Award), the Cincinnati Children's Research Foundation (Procter Scholar Award) to A.A., and NIH R01DK107530 and NIH R01DK123181 to T.N.

Received: January 6, 2020
Revised: December 13, 2020
Accepted: December 14, 2020
Published: January 14, 2021

REFERENCES

Alrefai, W.A., and Gill, R.K. (2007). Bile acid transporters: structure, function, regulation and pathophysiological implications. Pharm. Res. *24*, 1803–1823.

Asai, A., Aihara, E., Watson, C., Mourya, R., Mizuochi, T., Shivakumar, P., Phelan, K., Mayhew, C., Helmrath, M., Takebe, T., et al. (2017). Paracrine signals regulate human liver organoid maturation from induced pluripotent stem cells. Development *144*, 1056–1064.

Ballatori, N., Li, N., Fang, F., Boyer, J.L., Christian, W.V., and Hammond, C.L. (2009). OST alpha-OST beta: a key membrane transporter of bile acids and conjugated steroids. Front. Biosci Landmark Ed *14*, 2829–2844.

Ballatori, N., Christian, W.V., Wheeler, S.G., and Hammond, C.L. (2013). The heteromeric organic solute transporter, OSTα–OSTβ/SLC51: a transporter for steroid-derived molecules. Mol. Aspects Med. *34*, 683–692.

Bove, K.E., Heubi, J.E., Balistreri, W.F., and Setchell, K.D.R. (2004). Bile acid synthetic defects and liver disease: a comprehensive Review. Pediatr. Dev. Pathol. *7*, 315–334.

Briz, O., Romero, M.R., Martinez-Becerra, P., Macias, R.I.R., Perez, M.J., Jimenez, F., Martin, F.G.S., and Marin, J.J.G. (2006). OATP8/1B3-mediated Cotransport of Bile Acids and Glutathione an export pathway for organic anions from hepatocytes? J. Biol. Chem. *281*, 30326–30335.

Bruyn, T.D., Fattah, S., Stieger, B., Augustijns, P., and Annaert, P. (2011). Sodium fluorescein is a probe substrate for hepatic drug

transport mediated by OATP1B1 and OATP1B3. J. Pharm. Sci. *100*, 5018–5030.

Cheung, L., Flemming, C.L., Watt, F., Masada, N., Yu, D.M., Huynh, T., Conseil, G., Tivnan, A., Polinsky, A., Gudkov, A.V., et al. (2014). High-throughput screening identifies Ceefourin 1 and Ceefourin 2 as highly selective inhibitors of multidrug resistance protein 4 (MRP4). Biochem. Pharmacol. *91*, 97–108.

Christian, W.V., Li, N., Hinkle, P.M., and Ballatori, N. (2012). β-Subunit of the ostα-Ostβ organic solute transporter is required not only for heterodimerization and trafficking but also for function. J. Biol. Chem. *287*, 21233–21243.

Ellis, J.L., Bove, K.E., Schuetz, E.G., Leino, D., Valencia, C.A., Schuetz, J.D., Miethke, A., and Yin, C. (2018). Zebrafish abcb11b mutant reveals strategies to restore bile excretion impaired by bile salt export pump deficiency. Hepatology *67*, 1531–1545.

Imagawa, K., Takayama, K., Isoyama, S., Tanikawa, K., Shinkai, M., Harada, K., Tachibana, M., Sakurai, F., Noguchi, E., Hirata, K., et al. (2017). Generation of a bile salt export pump deficiency model using patient-specific induced pluripotent stem cell-derived hepatocyte-like cells. Sci. Rep. *7*, 41806.

Jansen, P.L., Strautnieks, S.S., Jacquemin, E., Hadchouel, M., Sokal, E.M., Hooiveld, G.J., Koning, J.H., Jager-Krikken, A.D., Kuipers, F., Stellaard, F., et al. (1999). Hepatocanalicular bile salt export pump deficiency in patients with progressive familial intrahepatic cholestasis. Gastroenterology *117*, 1370–1379.

Jones, D.E.J. (2016). Obeticholic acid for the treatment of primary biliary cirrhosis. Expert Rev. Gastroenterol. Hepatol. *10*, 1091–1099.

Keitel, V., Burdelski, M., Warskulat, U., Kühlkamp, T., Keppler, D., Häussinger, D., and Kubitz, R. (2005). Expression and localization of hepatobiliary transport proteins in progressive familial intrahepatic cholestasis. Hepatology *41*, 1160–1172.

Kenna, J.G., Stahl, S.H., Eakins, J.A., Foster, A.J., Andersson, L.C., Bergare, J., Billger, M., Elebring, M., Elmore, C.S., and Thompson, R.A. (2015). Multiple compound-related adverse properties contribute to liver injury caused by endothelin receptor antagonists. J. Pharmacol. Exp. Ther. *352*, 281–290.

Malinen, M.M., Kauttonen, A., Beaudoin, J.J., Sjöstedt, N., Honkakoski, P., and Brouwer, K.L.R. (2018). Novel in vitro method reveals drugs that inhibit organic solute transporter Alpha/Beta (OSTα/β). Mol. Pharm. *16*, 238–246.

Mennone, A., Soroka, C.J., Cai, S., Harry, K., Adachi, M., Hagey, L., Schuetz, J.D., and Boyer, J.L. (2006). Mrp4−/− mice have an impaired cytoprotective response in obstructive cholestasis. Hepatology *43*, 1013–1021.

Morotti, R., Suchy, F., and Magid, M. (2011). Progressive familial intrahepatic cholestasis (PFIC) type 1, 2, and 3: a Review of the liver pathology findings. Semin. Liver Dis. *31*, 003–010.

Nicolaou, M., Andress, E.J., Zolnerciks, J.K., Dixon, P.H., Williamson, C., and Linton, K.J. (2012). Canalicular ABC transporters and liver disease. J. Pathol. *226*, 300–315.

Pan, Q., Zhang, X., Zhang, L., Cheng, Y., Zhao, N., Li, F., Zhou, X., Chen, S., Li, J., Xu, S., et al. (2018). Solute carrier organic anion transporter family member 3A1 is a bile acid efflux transporter in cholestasis. Gastroenterology *155*, 1578–1592.e16.

Qiu, X., Zhang, Y., Liu, T., Shen, H., Xiao, Y., Bourner, M.J., Pratt, J.R., Thompson, D.C., Marathe, P., Humphreys, G.W., et al. (2016). Disruption of BSEP function in HepaRG cells alters bile acid disposition and is a susceptive factor to drug-induced cholestatic injury. Mol. Pharm. *13*, 1206–1216.

Strautnieks, S.S., Bull, L.N., Knisely, A.S., Kocoshis, S.A., Dahl, N., Arnell, H., Sokal, E., Dahan, K., Childs, S., Ling, V., et al. (1998). A gene encoding a liver-specific ABC transporter is mutated in progressive familial intrahepatic cholestasis. Nat. Genet. *20*, 233–238.

Strautnieks, S.S., Byrne, J.A., Pawlikowska, L., Cebecauerová, D., Rayner, A., Dutton, L., Meier, Y., Antoniou, A., Stieger, B., Arnell, H., et al. (2008). Severe bile salt export pump deficiency: 82 different ABCB11 mutations in 109 families. Gastroenterology *134*, 1203–1214.e8.

Takayama, K., Akita, N., Mimura, N., Akahira, R., Taniguchi, Y., Ikeda, M., Sakurai, F., Ohara, O., Morio, T., Sekiguchi, K., et al. (2017). Generation of safe and therapeutically effective human induced pluripotent stem cell-derived hepatocyte-like cells for regenerative medicine. Hepatol. Commun. *1*, 1058–1069.

Wang, R., Lam, P., Liu, L., Forrest, D., Yousef, I.M., Mignault, D., Phillips, J.M., and Ling, V. (2003). Severe cholestasis induced by cholic acid feeding in knockout mice of sister of P-glycoprotein. Hepatology *38*, 1489–1499.

Zollner, G., Wagner, M., Fickert, P., Silbert, D., Gumhold, J., Zatloukal, K., Denk, H., and Trauner, M. (2007). Expression of bile acid synthesis and detoxification enzymes and the alternative bile acid efflux pump MRP4 in patients with primary biliary cirrhosis. Liver Int. *27*, 920–929.